JOURNAL OF MATERIALS SCIENCE **36** (2001) 5017–5025

Zn-*K* EXAFS investigations on ZnS/ZnO containing vitrified ashes from municipal incinerator facilities

G. MOSEL, TH. HÜBERT, M. NOFZ, R. BRENNEIS, P. KÖCHER, G. KLEY
Federal Institute for Materials Research and Testing (BAM), Unter den Eichen 44-46, D-12203 Berlin, Germany
E-mail: thomas.huebert@bam.de

Zn-*K* transmission EXAFS measurements were performed on vitrified ashes from municipal waste incinerator facilities, which contain low amounts of Zn (up to 3 wt%) and sulphur (up to 0.5 wt%) in a ZnS phase. From the Fourier transform it can be concluded that the zinc ions are fourfold co-ordinated by oxygen or sulphur ions. The amount of zinc ions of sulphur environment, e.g. the concentration of ZnS, was determined by Fourier filtering and subsequent parameter fitting. A quantitative analysis of low ZnS concentrations up to 1 wt% has been performed for samples with a molar ratio Zn/S < 5.

1. Introduction

During the incineration of municipal waste the toxics become concentrated in the residual fly ash. Vitrification of the ash is widely considered to be the best processing option. The vitrification according to the RedMelt® process in an electric arc furnace causes thermal degradation of the toxic organics and a separation of the heavy metals and/or heavy metal compounds from the bulk material. The remaining bulk material is in the form of an inert vitrified product [1].

Under special melting conditions zinc may partly react with sulphur which appears in the ashes, leading to the formation of zinc sulphide (ZnS) and ZnS/FeS alloys. The presence of these phases, even in small quantities, deteriorates the mechanical properties of the final material and prevents its further application as construction material. On the other hand these small ZnS and/or ZnS/FeS particles may act as crystallisation centres and can facilitate the formation of glass ceramics. Therefore, it is important to investigate the relation between the concentration of reductants in the electric arc furnace and the Zn content as well as the local environment of the Zn ions, consisting of S or O ions in the bulk material. An analogous analysis of the Fe co-ordination was performed recently by means of Mössbauer spectroscopy [2].

In this study, vitrified ashes from municipal waste incinerator facilities, which contain low amounts of Zn (up to 3 wt%) and sulphur (up to 0.5 wt%), have been investigated. Because of these low concentrations and the presence of ferrous sulphide, the Zn environment cannot be investigated by X-ray diffraction. Thus, extended X-ray absorption fine structure spectroscopy (EXAFS) as a chemically selective method was chosen to investigate the local structure of the Zn ions. Transmission EXAFS measurements at the Zn-*K* edge were performed to determine the amount of Zn ions surrounded either by sulphur or oxygen atoms in a zinc sulphide or zinc silicate phase of the vitrified ashes.

2. Experimental procedure

2.1. Ash-derived glasses and reference samples

16 samples of vitrified ashes and ash mixtures have been investigated. Their chemical compositions, given in Table I, were determined by X-ray fluorescence analysis. According to the Zn/S molar ratio the samples are divided in two groups (Zn/S molar ratio less or greater than 2). The sample TK 1923 is a sulphur-free reference glass. As further reference materials, polycrystalline ZnO, Zn_2SiO_4 (willemite) and ZnS were selected. Additionally, a series of xZnO-$(100-x)$ZnS mixtures covering the whole composition range in steps of 20 mol%, i.e. $x = 0, 20, 40, 60, 80, 100$, was prepared.

2.2. EXAFS spectroscopy

Calculations of the signal-to-background and signal-to-noise ratios as well as test measurements on three samples at HASYLAB (Hamburg) [3] revealed that quantitatively analysable Zn-*K* EXAFS spectra can be collected in transmission mode down to Zn contents of about 0.1 wt% using a synchrotron radiation (SR) source with a photon flux of 10^9 to 10^{10} s^{-1} in a time of about 20 min per spectrum. Favourable conditions are available at beamline BL18 of the European Synchrotron Radiation Facility (ESRF) in Grenoble. 16 glassy samples and 7 reference samples were investigated at BL18 using a Si-(311) monochromator which delivers a very high and nearly constant photon flux

TABLE I Composition of the vitrified samples (concentrations in wt%) and Zn/S molar ratio

Group	Sample	Zn/S ratio	Zn	S	Si	Al	Ca	Mg	Na	K	Fe
A	TK 1963	0.15	0.06	0.20	23.6	8.8	10.0	1.6	3.1	1.0	4.2
	TK 1959	0.26	0.10	0.19	23.6	8.5	10.0	1.6	3.2	1.0	4.5
	TK 2163	0.34	0.22	0.32	21.4	5.2	16.7	2.2	2.1	1.30	1.9
	TK 2123	0.45	0.42	0.46	19.9	5.0	19.4	5.4	2.0	0.62	2.0
	TK 2181	0.53	0.43	0.40	23.2	5.4	17.6	2.0	2.0	1.00	2.0
	TK 1956	0.54	0.165	0.15	23.0	8.5	9.7	1.6	3.2	1.0	5.2
	TK 2128	0.94	0.73	0.38	19.8	5.1	19.2	5.2	2.0	0.6	2.2
	TK 2220	1.09	0.62	0.28	23.7	5.3	16.3	2.0	2.3	1.40	2.4
	TK 2193	1.36	0.61	0.22	23.7	4.7	14.7	1.8	2.2	1.30	2.3
B	TK 2021	3.76	0.92	0.12	20.5	9.2	10.5	2.6	1.9	1.8	6.8
	TK 2117	5.14	2.2	0.21	17.5	4.7	20.3	5.9	2.2	0.5	3.2
	TK 2151	8.36	1.5	0.088	23.1	4.3	16.0	1.5	2.2	1.0	2.7
	TK 2145	10.4	2.1	0.099	23.3	4.2	15.2	1.4	2.4	1.1	3.1
	TK 2110	20.1	1.8	0.044	18.6	4.6	18.9	5.5	2.9	0.7	3.0
	TK 2042	20.7	3.0	0.071	17.4	4.7	18.5	5.6	3.5	0.9	3.0
	TK 1923	—	0.97	0	20.6	10.4	16.9	1.8	1.6	0	0.7

in the spectral range of the Zn-K edge (9400 eV to 10200 eV).

2.2.1. EXAFS samples

Samples for transmission EXAFS must fulfil two main requirements, (i) homogeneity and (ii) thickness close to the optimum thickness ($\mu \cdot d_{\text{opt}} = 2.55$) [4]. For the samples in Table I d_{opt} is (280 ± 40) μm.

Three preparation techniques were used to meet these requirements.

a) Using silk-screen printing, thin layers on polypropylene foil were prepared from powders with a grain size of $d_{50} \approx 5$ μm. The thickness of a single layer is about 40 μm. Homogeneous samples with thicknesses close to d_{opt} were obtained by stacking 8 to 16 layers one after another. This method was used for all samples.

b) For 6 glasses thin polished sections were prepared. These bulk samples were free of pinholes and were expected to show very good homogeneity.

c) Several glassy samples were prepared as pellets. The minimum thickness possible was about 400 μm, i.e. somewhat larger than d_{opt}.

During the EXAFS measurements it was found that samples prepared using techniques a) and b) give spectra with sufficient signal-to-noise ratio and reproducible EXAFS amplitudes. The pellets (method c), however, showed serious inhomogeneities. The data analysis was restricted to samples prepared by silk-screen printing.

2.2.2. Primary data analysis

The steps of the primary data analysis of a typical EXAFS spectrum are shown in Fig. 1(a–f). Fig. 1a presents the measured Zn-K EXAFS spectrum. The background which is not related to absorption processes in the Zn-K edge is calculated by extrapolating the pre-edge range (Victoreen fit). The spectrum given in Fig. 1b results after background subtraction. Fig. 1c shows the EXAFS range of the absorption spectrum $\mu(E)$, i.e. the absorption coefficient μ as a function of the energy E_{Ph} of the photoelectron emitted during the absorption process in the Zn-K shell. The backscattering of this photoelectron by the neighbouring atoms delivers information on the distance, co-ordination number and disorder in the nearest co-ordination shells of the absorbing Zn atoms. The dotted curve, the function $\mu_0(E)$, which was calculated using a suitable cubic spline fit, approximately represents the so-called "undistorted absorption", which would appear in the case of isolated Zn atoms. Applying the formula $\chi(E) = (\mu(E) - \mu_0(E))/\mu_0(E)$ the EXAFS modulation $\chi(E)$ is calculated. Performing the transformation from the energy E of the emitted photoelectron to its wavelength $k = 8\pi^2 m(E - E_0)^{1/2}$ and applying the weighting factor k the EXAFS modulation $k \cdot \chi(k)$ (Fig. 1d) is determined. Usually a k^3 weighting is applied resulting in the function $k^3 \cdot \chi(k)$ (straight line in Fig. 1e). The Fourier transform of $k^3 \cdot \chi(k)$ delivers the complex function $F(r)$. Its modulus $|F(r)|$ given in Fig. 1f is dominated by a main peak between 1 and 2 Å, which contains the structural information on the first co-ordination shell of the Zn atoms. Inverse Fourier transformation of this peak results in the Fourier-filtered EXAFS modulation $k^3 \cdot \chi_1(k)$ (dotted line in Fig. 1e). The index 1 indicates that this function contains only the information related to the first co-ordination of the Zn atoms. The function $k^3 \cdot \chi_1(k)$ can be analysed by parameter fitting as explained in the following section. Detailed descriptions of the primary data analysis are given in [3, 4].

2.2.3. Parameter fitting

The analysis of an EXAFS spectrum comprises a qualitative description of the Fourier transform and a subsequent parameter fitting of a theoretical model function $k \cdot \chi_{\text{th}}(k)$ to the experimentally obtained function $k \cdot \chi(k)$. The model function $k \cdot \chi_{\text{th}}(k)$, which corresponds to the structure factor in X-ray diffraction, can be calculated using the EXAFS equation (1), which describes the EXAFS modulation as a superposition of the backscattering contributions of the co-ordination shells j around the absorbing atomic species (here Zn).

$$k \cdot \chi_{th}(k) = -\sum_j \frac{N_j}{R_j^2} S_0^2(k) \cdot f_j(k, \pi) \cdot \exp\left(-2\sigma_j^2 k^2\right) \cdot \exp\frac{-2(R_j - \Delta)}{\lambda(k)} \cdot \sin(2kR_j + \varphi_j(k)) \quad (1)$$

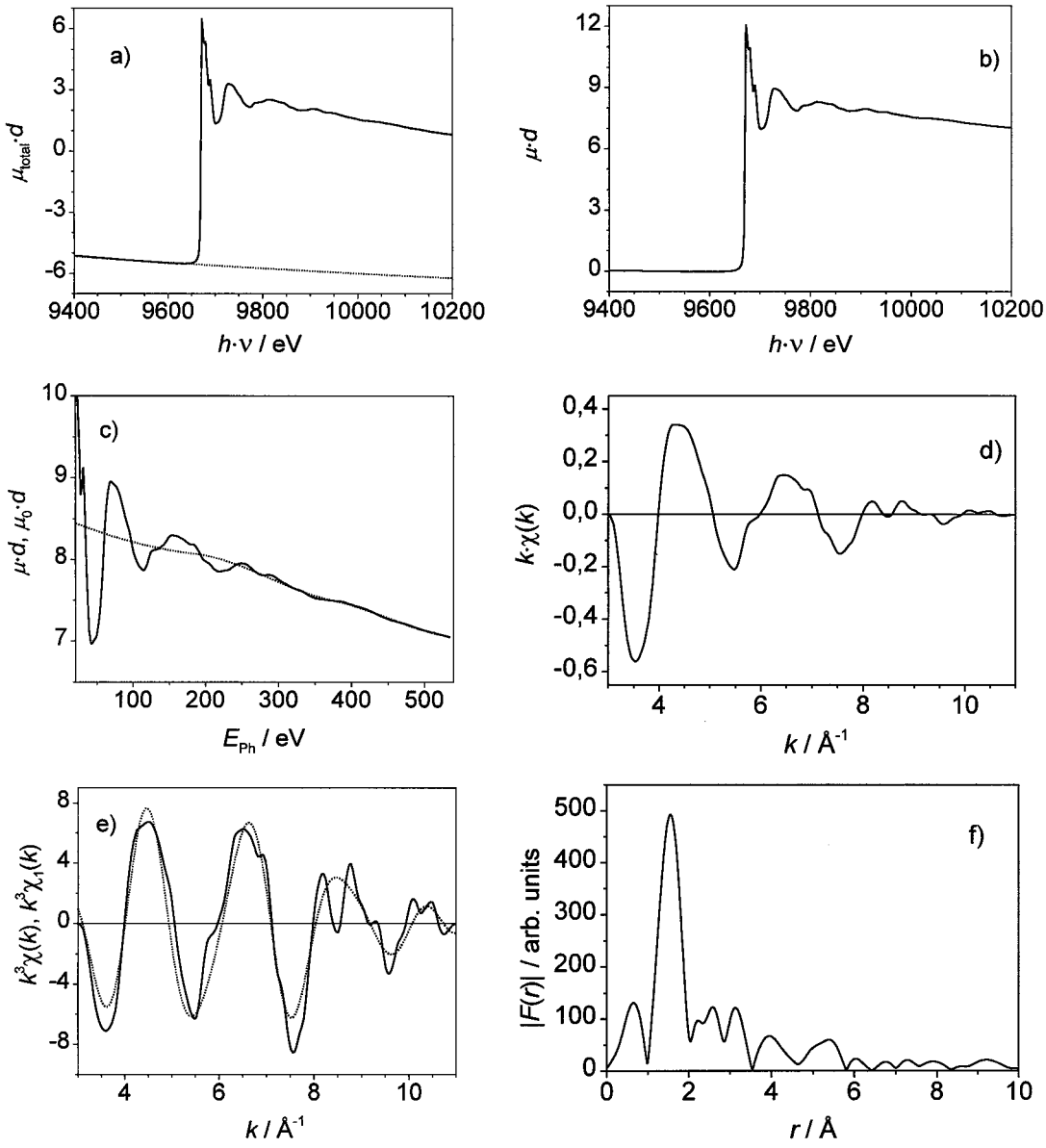

Figure 1 Primary data analysis of EXAFS spectrum.

It contains the following structural parameters: the mean interatomic distance R_j between the absorbing atom and the backscattering atoms in the j-th shell, the co-ordination number N_j, and the mean square deviation σ_j^2, a measure for the disorder in the j-th shell. To obtain the initial model function for the fit, suitable starting values for these parameters have to be chosen.

Quantitative analysis is possible under the prerequisite that the backscattering amplitudes $f_j(k, \pi)$ and the scattering phase shifts $\varphi_j(k)$, which describe the scattering behaviour of the system absorber atom - backscatterer atom, and the mean free path $\lambda(k)$ of the photoelectron are known. These data have to be determined from reference spectra of suitable crystalline samples with well-known structures. In this work, the reference spectra from willemite (Zn_2SiO_4) and ZnS have been used to determine the functions f, φ and λ for the scattering systems Zn-O and Zn-S, respectively. Because of the limited mean free path of the photoelectron the structural information is restricted to the local environment, i.e. up to a radial distance of about 5 Å in the case of crystalline samples. For most amorphous samples the structural information is limited to the first co-ordination shell. Thus, the sum over j is reduced to the contribution $j = 1$. The applied Fourier-filtering of the experimental EXAFS modulation suppresses the weak contributions from atoms beyond the first co-ordination shell.

During the fit the structural parameters R_1, N_1, and σ_1^2 are refined applying a least-squares procedure until an optimum coincidence between theoretical and experimental function is obtained.

3. Results and discussion

3.1. Polycrystalline reference samples

In Fig. 2 the EXAFS modulations $k^3 \cdot \chi(k)$ and the Fourier transforms $|F(r)|$ of the polycrystalline references ZnO, Zn_2SiO_4 (willemite) and ZnS are given. The substances contain Zn^{2+} ions in tetrahedral co-ordination of O^{2-} or S^{2-} ions [5–7]. The Fourier transforms of the mixtures of polycrystalline ZnO and ZnS references presented in Fig. 3 show that Zn ions in oxide

and sulphide environments can be easily distinguished by the different distances to the anion ($R_{Zn-O} = 1.98$ Å, $R_{Zn-S} = 2.34$ Å) which give peaks with maxima at 1.59 Å and 1.95 Å, respectively. This difference between the peak positions in the $|F(r)|$ and the real distances known from XRD is typical for EXAFS. It is caused by the scattering phase shift of the emitted photoelectron at the potentials of the absorber and the neighbouring atoms.

With increasing ZnO concentration the peak at 1.95 Å diminishes whereas the peak at 1.59 Å rises. At intermediate concentrations a typical double peak structure is visible in the range 1.0 Å $< r <$ 2.5 Å. In the range 2.5 Å $< r <$ 5.0 Å further peaks are visible which correspond to the second and third co-ordination shell of the Zn ions. These peaks are more intense for ZnO than for ZnS, despite both compounds possess the wurtzite structure.

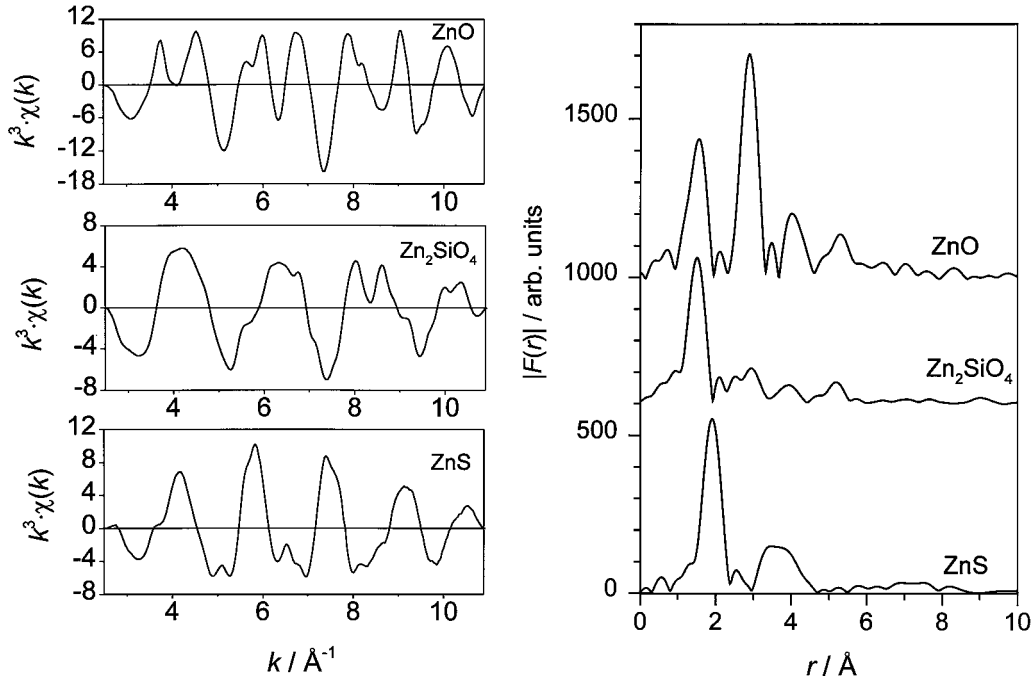

Figure 2 EXAFS modulations $k^3 \cdot \chi(k)$ and the Fourier transforms $|F(r)|$ of the polycrystalline references ZnO, Zn_2SiO_4 (willemite) and ZnS.

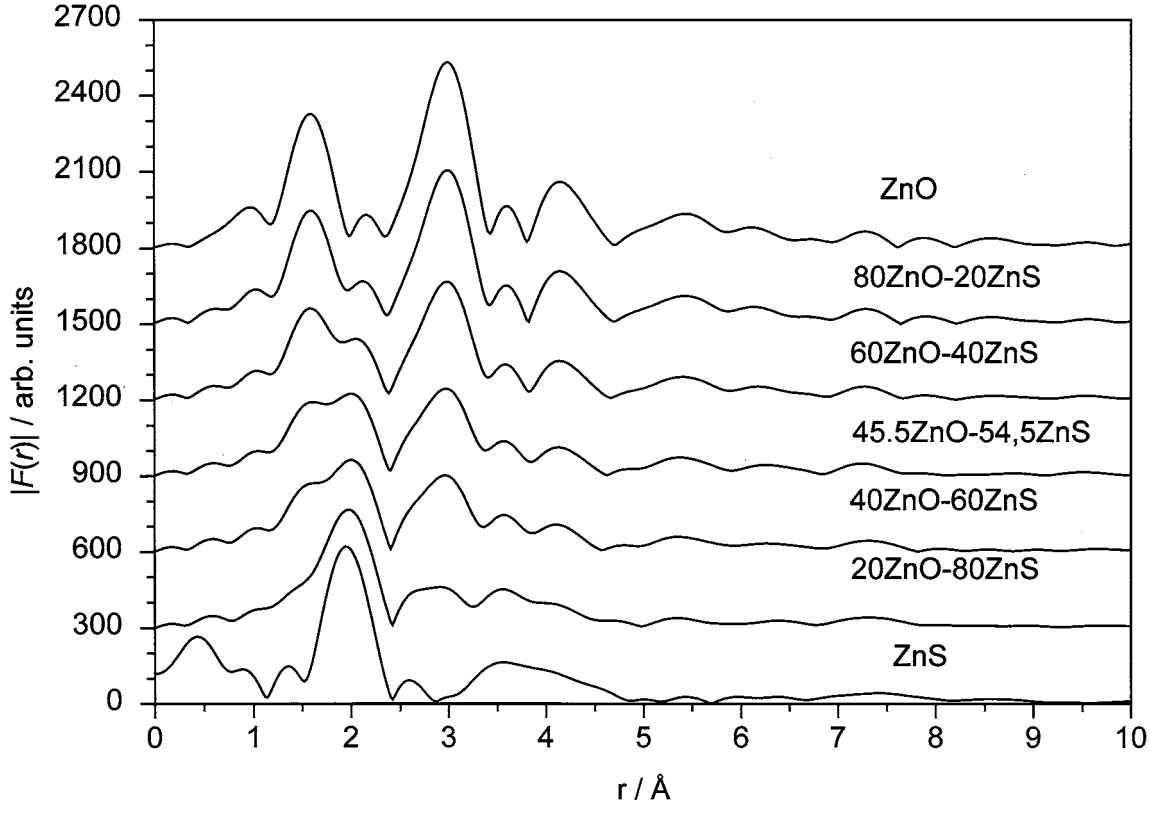

Figure 3 Fourier transforms of reference mixtures of polycrystalline ZnS and ZnO.

TABLE II Zn co-ordination in ZnS (wurtzite structure) and ZnO

	Bond lengths in Å	
Shell	ZnS	ZnO
1	2.34 (4 S)	1.98 (4 O)
2a	3.82 (12 Zn)	3.23 (12 Zn)
2b	3.91 (1S)	3.25 (1 O)
3	4.48 (9 S)	3.80 (9 O)

(Data taken from literature [6–8].)

Table II presents structural parameters up to the third co-ordination shell obtained by diffraction methods (taken from [6–8]).

The usability of the scattering data for the quantitative detection of the amount of Zn atoms in sulphidic and oxidic environments, respectively, was tested analysing the spectra of the ZnO/ZnS mixtures ($x = 20 \ldots 80$) via parameter fitting. The procedure differs somewhat from the typical EXAFS fitting described in Section 2. It is assumed that a Zn atom may appear either in an oxidic or in a sulphidic environment with the first co-ordination shell as in crystalline ZnO and ZnS, respectively. This assumption is based on the fact that there is a large difference in zinc-oxygen and zinc-sulphur bond lengths and that no crystalline zinc oxysulphides are known. In the model function a linear superposition of the backscattering effect on Zn atoms in sulphidic and oxidic environments is applied. This function is fitted to the experimental spectra varying the weighting factors p_{ZnO} and p_{ZnS}, whereas the values R_1, N_1, and σ_1^2 were fixed. The values p_{ZnO} and p_{ZnS} correspond to the percentages of Zn atoms in the two assumed environments. The results in Table III show a good coincidence to the real sample composition c_{ZnO} and c_{ZnS}. As the sum $p_{ZnO} + p_{ZnS}$ deviates slightly from the ideal value of 100 mol% the results were normalised using the formula $P_j = (p_j / \Sigma p_i) \cdot 100\%$.

3.2. Vitrified ashes

3.2.1. Group A samples

The EXAFS modulations $k^3 \cdot \chi(k)$ and Fourier transforms $|F(r)|$ of the ash samples are shown in Figs 4 and 5. For comparison the $|F(r)|$ of ZnS and ZnO are given. All $|F(r)|$ were calculated using the interval $3\ \text{Å}^{-1} < k < 11\text{Å}^{-1}$. The samples TK 1963, 1959 and 1956 had to be excluded from the further analysis, because the signal-to-noise ratio was very low due to the small Zn concentration (0.060 to 0.165 wt%).

The signal-to-noise ratio of the EXAFS modulations $k^3 \cdot \chi(k)$ in Fig. 4 allows a quantitative analysis. The glitch at 9.6 Å^{-1} should not lead to significant errors.

TABLE III Results of the parameter fit of the xZnO-(100–x)ZnS mixtures

Real composition		Results of parameter fit		Normalised results	
C_{ZnO}/mol%	C_{ZnS}/mol%	p_{ZnO}/mol%	p_{ZnS}/mol%	P_{ZnO}/mol%	P_{ZnS}/mol%
0	100	0	100	0	100
20	80	22.2	78.4	22.1	77.9
40	60	41.1	60.5	40.6	59.4
60	40	64.5	38.6	62.6	37.4
80	20	83.1	20.9	79.9	20.1
100	0	100	0	100	0

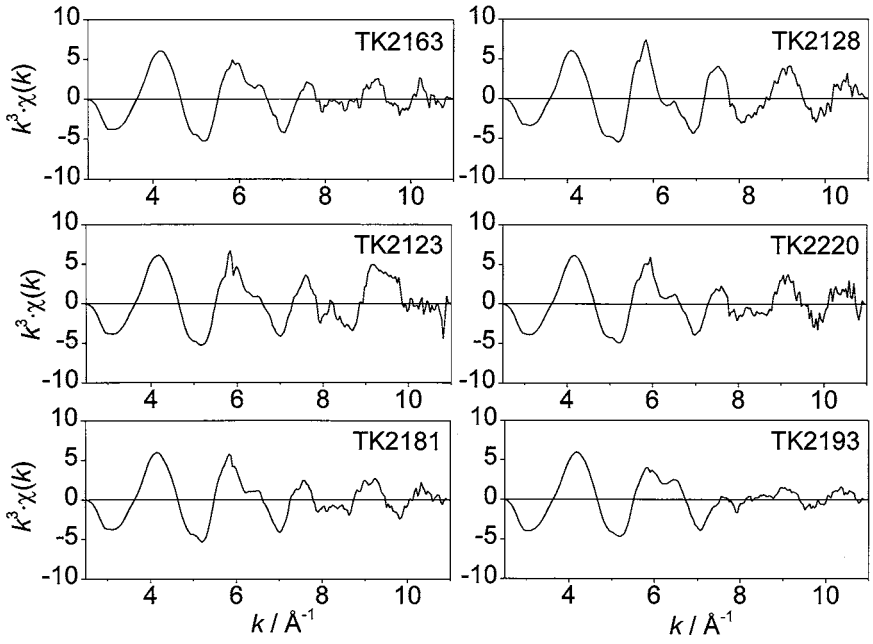

Figure 4 EXAFS modulations $k^3 \cdot \chi(k)$ of the samples of group A.

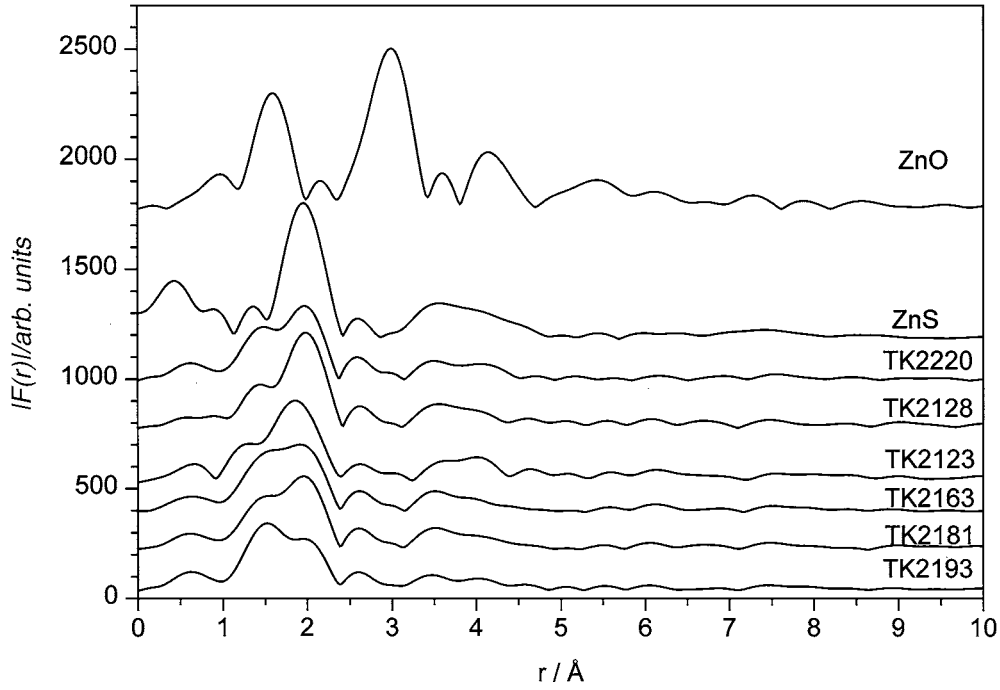

Figure 5 Fourier transforms $|F(r)|$ of the samples of group A compared to those of the reference compounds ZnS and ZnO.

The $|F(r)|$ of the samples of the vitrified ashes with low Zn content show a characteristic double peak structure in the range 1.0 Å $< r <$ 2.5 Å, similar to those of the reference mixtures (Fig. 2). The intensities of both subpeaks (maxima at about 1.60 Å and 1.95 Å) vary considerably within the investigated sample series. Additional structures are visible in the $|F(r)|$ between 2.5 Å and 5.0 Å, which are very similar to those of polycrystalline ZnS, whereas no ZnO-like features appear. This indicates that the Zn ions co-ordinated with sulphur from ZnS crystallites, whereas the Zn ions in oxidic environment remain in a disordered silicate environment, without formation of crystalline ZnO particles.

The part of the first co-ordination shell of the spectra can be separated by an inverse Fourier transformation in the range of 0.7 Å $< r <$ 2.6 Å. The resulting Fourier-filtered EXAFS modulation $k_1 \cdot \chi(k)$ was analysed by parameter fitting assuming a superposition of the contributions of ZnO_4 and ZnS_4 tetrahedra, i.e. only the model function which has been tested successfully in Section 3.1. In order to reduce the number of free parameters, the following assumptions were made:

i. The Zn^{2+} ions of oxidic and sulphidic environments in the samples have tetrahedral co-ordination and the zinc-anion distances and the mean square deviations differ only slightly.

ii. A mixed co-ordination of one zinc ion by oxygen and sulphur ions, i.e. the formation of oxysulphides, is excluded.

Thus, free parameters are only the quantitative amounts of zinc ions p_{Zn-O} und p_{Zn-S} in oxygen and sulphur environment. In a first fit, the experimental scattering functions of ZnO and ZnS were used for the estimation of the EXAFS model functions $k \cdot \chi_{th}(k)$. In a second fit, the scattering function of willemite (Zn_2SiO_4) instead of ZnO was used, because of the similar silicate environment. As above, the values for R_1, N_1, and σ_1^2 in oxidic and sulphidic environment were fixed. The model was restricted to the first co-ordination shell made up by either four oxygen ions or four sulphur ions. The model function was fitted to the experimental Fourier-filtered function $k \cdot \chi_1(k)$ by varying only the parameters p_{ZnO} and p_{ZnS}, which represent the percentages of Zn ions in oxide and sulphide environment, respectively. The results of both fits, given in Table IV, are very similar.

The residue is the sum of the squared differences between the experimental and the model function divided by the number of measuring points. The lower the residuum the better the fit quality. The results of both fits were combined and normalised by the sum $p_{Zn-O} + p_{Zn-S}$. The resulting amount of zinc ions with sulphidic environment (called P_{Zn-S}) should be strongly influenced by the molar Zn/S ratio, what hides

TABLE IV Results of parameter fit

		First fit (ZnO and ZnS)			Second fit (Willemite and ZnS)		
Sample	Zn/S	p_{Zn-O}	p_{Zn-S}	Residue	p_{Zn-O}	p_{Zn-S}	Residue
TK2163	0.34	0.54	0.43	1.41	0.55	0.43	0.942
TK2123	0.43	0.46	0.52	4.21	0.48	0.51	3.91
TK2181	0.53	0.47	0.49	1.12	0.47	0.48	0.903
TK2128	0.91	0.30	0.68	0.981	0.31	0.67	1.11
TK2220	1.09	0.48	0.48	1.73	0.48	0.47	1.72
TK2193	1.35	0.62	0.32	1.08	0.56	0.35	0.538

the influence of the reaction conditions. Therefore the amount P_{Zn-S} was multiplied by the Zn/S ratio. The resulting $P_{Zn-S,fictive}$ gives the amount of sulphur co-ordinated zinc of a fictive sample of the Zn/S ratio = 1. The results in Table V show that this amount is lower than P_{Zn-S} and can be correlated to the kind and concentration of added reducing additives. From the samples treated with 2 wt% reductant it is visible that the ZnS concentration is lower (by a factor of nearly 3), if SiC instead of carbon is used as reductant. With increasing SiC content the ZnS concentration is clearly reduced. These results indicate that the formation of the ZnS phase can be avoided when SiC instead of carbon is used as reductant. Probably SiC leads to the formation of additional zinc silicate, whereas carbon promotes the reduction of sulphates from the ashes to sulphides in the melts.

TABLE V Results of estimation of zinc ions in sulphur environment

Sample	Zn/S	P_{Zn-S}/%	$P_{Zn-S,fictive}$/%	Reductant
TK2163	0.34	0.44 ± 0.10	0.15 ± 0.04	3 wt.% SiC
TK2123	0.43	0.52 ± 0.10	0.23 ± 0.04	2 wt.% SiC
TK2181	0.53	0.50 ± 0.10	0.26 ± 0.05	2 wt.% SiC
TK2220	1.09	0.50 ± 0.10	0.54 ± 0.11	1 wt.% SiC
TK2193	1.35	0.34 ± 0.10	0.46 ± 0.13	1 wt.% SiC
TK2128	0.91	0.69 ± 0.10	0.63 ± 0.09	2 wt.% C

3.2.2. Group B samples

The EXAFS modulations $k^3 \cdot \chi(k)$ and Fourier transforms $|F(r)|$ of the samples are shown in Figs 6 and 7. The functions $k^3 \cdot \chi(k)$ are dominated by only one

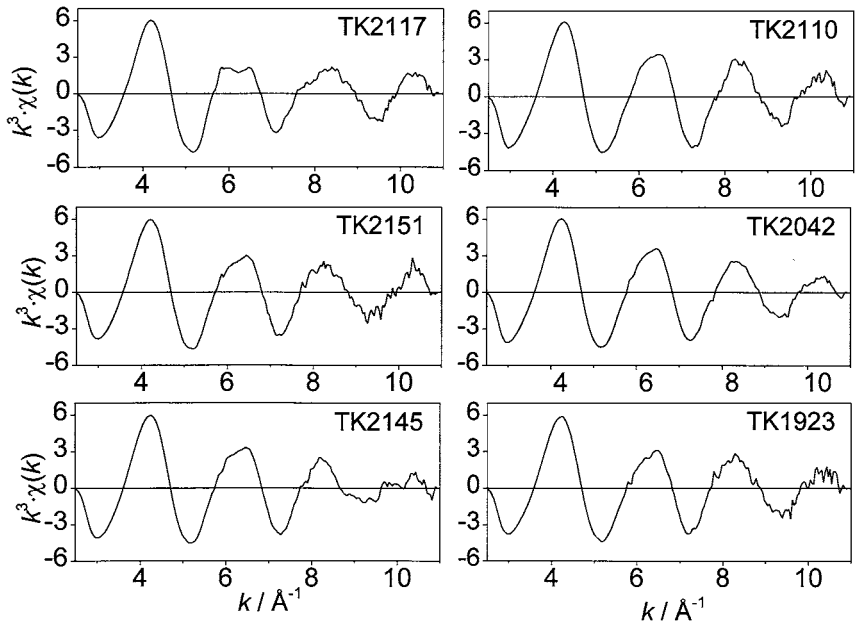

Figure 6 EXAFS modulations $k^3 \cdot \chi(k)$ of the samples of group B.

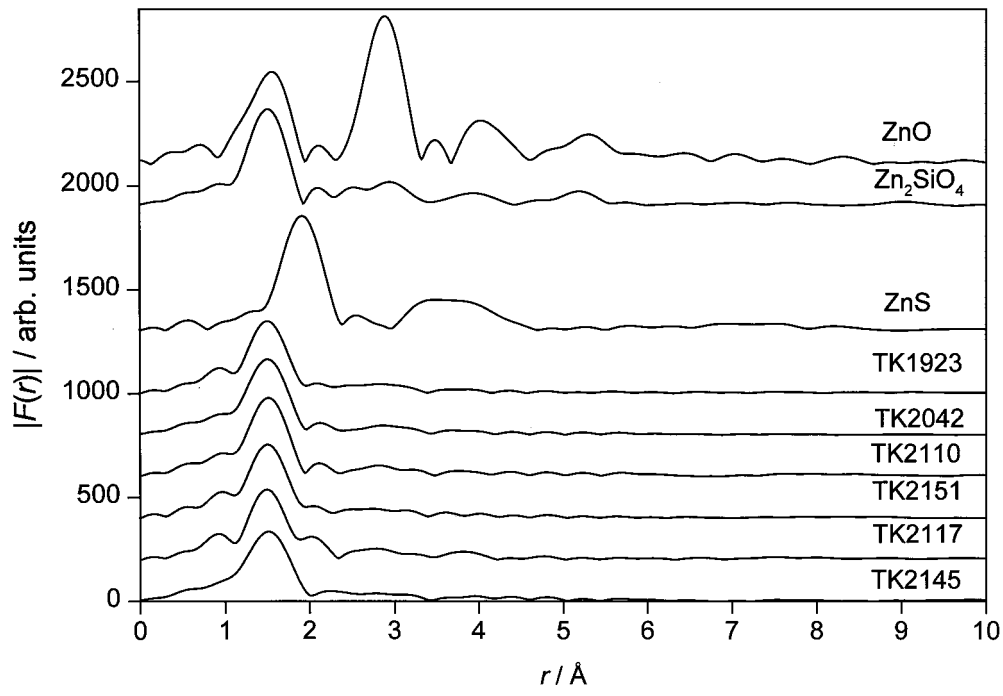

Figure 7 Fourier transforms $|F(r)|$ of the samples of group B compared to those of the reference compounds ZnS and ZnO.

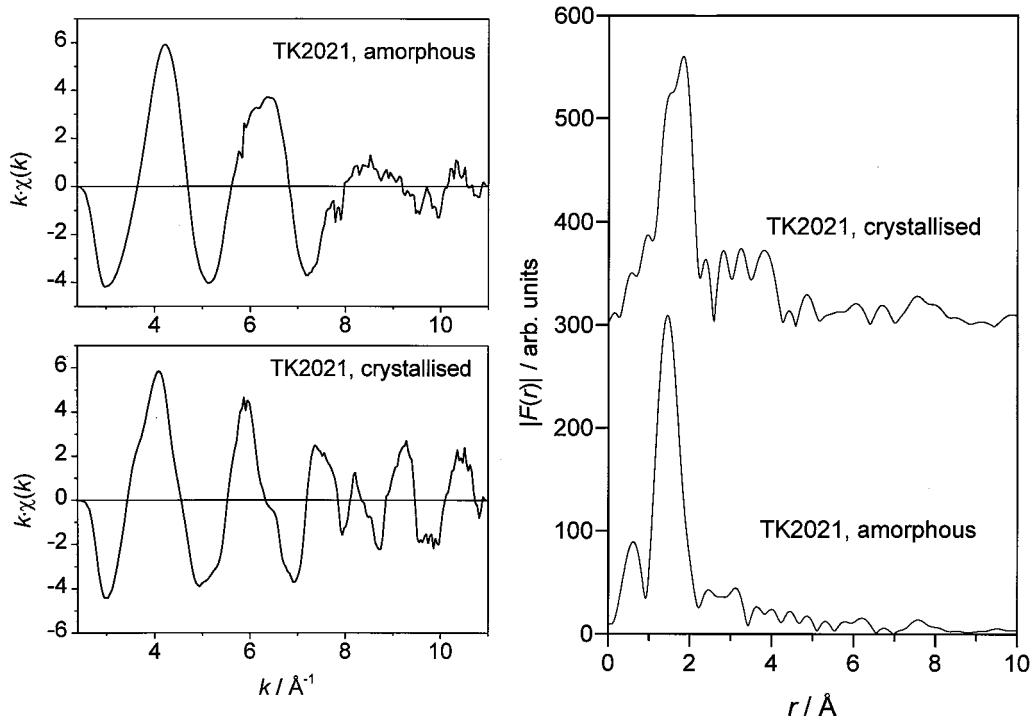

Figure 8 EXAFS-modulations $k^3 \cdot \chi(k)$ and Fourier transforms $|F(r)|$ of sample TK2021 (vitreous and crystalline).

oscillation, in contrast to the more complicated shape of those of group A (Fig. 4). No structures related to crystalline ZnS are visible.

The simple structure of the EXAFS modulations is reflected in the Fourier transforms, which are dominated by a single peak (maximum at about 1.6 Å) due to Zn ions in oxidic environment. The structure related to Zn in sulphidic environment (sub-peak at 1.95 Å) appears only as a weak shoulder at 2.0 Å in the $|F(r)|$ of the samples TK 2117 and TK 2151. It is absent for the samples TK 1923, TK 2042, TK 2110 and TK 2145. However, this result does not exclude the formation of ZnS in these samples. The decisive parameter, which determines the shape of the Fourier transforms, is the high Zn/S molar ratio (Table I). Because of the lack of sulphur only a small percentage of the Zn ions can be co-ordinated by S ions. The remaining 90–95% must be in oxidic environment and therefore dominate the $|F(r)|$.

3.2.3. Crystallisation of ash-derived melts

The EXAFS modulations $k^3 \cdot \chi(k)$ and the Fourier transforms $|F(r)|$ of sample TK 2021 both as the vitrified ash and crystallized on slow cooling (~10 K/min) from the same melt are given in Fig. 8. The resulting main crystalline silicate phase is augite $Ca(Mg,Fe^{3+},Al)(Si,Al)_2O_6$ [9]. The $|F(r)|$ differ clearly from those of the three reference samples ZnO, ZnS and Zn_2SiO_4 (willemite). A comparison of the $k^3 \cdot \chi(k)$ of willemite and ZnS shows that both phases should be present. From the Fourier transform it is clear that the shape and position of the first co-ordination shell are changed significantly. The peak changes from a nearly symmetric shape of the vitrified samples to a double peak structure in the re-crystallised sample. The maximum at 1.5 Å—typical for the ZnO_4 group—changes to 1.9 Å (i.e. closer to the ZnS_4 group) and reduces its height.

In Table VI the results of the described parameter fit are given. The amount of zinc ions in a sulphur environment, $P_{Zn-S} = 0.46$, differs from the results given by the chemical analysis. From the molar ratio of 3.76, it can be concluded that only 25% of the zinc ions can be surrounded by sulphur. The residua of the fits are larger than those of the other fits. Therefore it can be concluded that the used model which considered only ZnO_4- and ZnS_4-groups is insufficient. It is possible that some of the zinc is six-fold co-ordinated and may be incorporated in the augite structure instead of magnesium what may cause the peak shift.

4. Conclusions

i. The zinc ions in vitrified ashes are surrounded by oxygen or sulphur ions in tetrahedral coordination.

ii. The zinc ions in the sulphidic environment are located in crystalline ZnS inclusions, whereas the zinc ions in the oxidic environment are incorporated in the amorphous silicate matrix.

TABLE VI Results of parameter fit

			First fit (ZnO and ZnS)			Second fit (Willemite, ZnS)		
Sample	Zn/S	P_{Zn-S}	P_{Zn-O}	P_{Zn-S}	Residuum	P_{Zn-O}	P_{Zn-S}	Residuum
TK2021 amorph.	3.76	0.16	0.75	0.14	2.18	0.73	0.15	3.18
TK2021 cryst.	3.76	0.46	0.50	0.45	9.49	0.51	0.42	4.95

iii. A quantitative determination of low amounts of ZnS ($\geq$1 wt%) can be performed if the Zn/S molar ratio is smaller than 5. At higher zinc concentrations the ZnS contribution to the EXAFS spectra is eclipsed by the contribution of the zinc ions of oxygen environment.

Acknowledgements

We are grateful to M. Borowski (E.S.R.F.) for experimental assistance. This work has been supported by the Deutsche Forschungsgemeinschaft (DFG) under contract Hu 491/2-2 and the Fonds der Chemischen Industrie (FCI).

References

1. G. KLEY, P. KÖCHER, A. FREUDENBERG and M. FAULSTICH, RedMelt®-Verfahren für oxidische Reststoffe aus Verbrennungs- und Industrieanlagen, Beiheft 31 zu "Müll und Abfall," Berlin, 1994, p. 146.
2. H. MEHNER and R. BRENNEIS, unpublished results.
3. G. MOSEL, M. NOFZ, TH. HÜBERT, R. BRENNEIS, P. KÖCHER and G. KLEY, HASYLAB Annual Report 1997, Part I, Hamburg, 833.
4. "X-Ray Absorption: Principles, Applications and Techniques of EXAFS, SEXAFS and XANES," edited by D. C. Koningsberger and R. Prins (Wiley Interscience, New York, 1988) p. 167.
5. K.-H. KLASKA, J. C. ECK and D. POHL, *Acta Cryst.* **B34** (1978) 3324.
6. E. H. KISI and M. M. ELCOMBE, *ibid.* **C45** (1989) 1867.
7. J. ALBERTSSON, S. C. ABRAHAMS and Å. KVICK, *ibid.* **B45** (1989) 34.
8. S. LINDROOS, Y. CHARREIRE, T. KANNIANINEN, M. LESKELÄ and S. BENAZETH, *J. Mater. Chem.* **7** (1997) 741.
9. J. CLARK, D. APPLEMAN and PAPIKE, *J. Mineral Soc. Am. Spec. Pap.* **2** (1969) 31.

Received 4 May 2000
and accepted 19 June 2001